



Ratiometric fluorometric and visual determination of cyanide based on the use of carbon dots and gold nanoclusters

Jing Wang¹ · Yu Qiu¹ · Daquan Li¹ · Xinyue Liu¹ · Chenxing Jiang¹ · Liang Huang¹ · Huimin Wen¹ · Jun Hu¹

Received: 9 April 2019 / Accepted: 7 September 2019 / Published online: 19 November 2019
© Springer-Verlag GmbH Austria, part of Springer Nature 2019

Abstract

An optical method is described for the ratiometric fluorometric determination of cyanide ions. It is based on the use of a mixture of aqueous solutions of blue-emitting carbon dots (CDs) and red-emitting gold nanoclusters (AuNCs). The presence of cyanide reduces the red fluorescence of the AuNCs through the formation of a stable complex $[\text{Au}(\text{CN})_2^-]$. The blue emission of the CDs, in contrast, stays constant. Hence, the color of fluorescence changes from red to purple to blue. The ratio of the fluorescence intensities located at 612 and 438 nm varies over a wide range, with 2 linear responses ranges (from 8 nM to 12.5 μM , and from 12.5 to 75 μM). The method was applied to the determination and visual discrimination of cyanide in food and drink samples.

Keywords Ratiometric determination · Visual discrimination · Cyanide nanoprobe · Two linear response ranges · Elsnier reaction · Stern–Volmer plot

Introduction

Cyanide is recognized as an extremely toxic chemical species to human health. The maximum acceptable concentration level of cyanide in drinking water is limited as 1.9 μM according to the World Health Organization [1, 2]. To date, numerous methods have been proposed to quantitatively detect cyanide, including photo-electrochemistry [3, 4], chemiluminescence [5], colorimetry [6, 7] and fluorescence [8, 9]. Compared with the other signal outputs, fluorescence techniques are particularly attractive as a result of their rapid response, high sensitivity, simple operation, and low cost. Organic fluorophores have been widely explored to monitor cyanide through specific coordination and chemical reactions [10, 11]. Although they always display superior selectivity and sensitivity, their complicated synthesis, poor photostability, and low water-solubility limit practical applications. In contrast, nanoparticles are more suitable to detect

cyanide in real samples because of their high stability and excellent water-solubility [12–14]. Literature survey shows that there is considerable interest in developing semiconductor quantum dots (QDs)-based nanoprobe for aqueous cyanide [15]. Nevertheless, most of the used QDs are inherent toxicity and their selectivity is still a challenge. As known, the bonding or reaction between the target and the surface of QDs is not specific enough and will be readily affected by its surround condition [16, 17].

Among the fluorescent nanoprobe, carbon dots (CDs) and noble metal nanoclusters have been regarded as potential candidates to replace conventional QDs due to their additional merits, such as low toxicity and strong photostability [18–21]. Some CDs or noble metal nanoclusters-based cyanide detectors have been reported. For instance, Liang et al. reported the highly luminescent nitrogen and sulfur co-doped CDs as a sensing platform for cyanide detection by fluorescent recovery [12]. Ying's group prepared the gold silver nanoclusters for sensitive detection of cyanide with a limit of detection of 138 nM and the probe had been successfully employed in cell imaging [22]. Chang and co-workers designed bovine serum albumin (BSA)-stabilized cerium/gold nanoclusters (Ce/AuNCs) with looser structures of the protein templates, which have the advantage of short detection time of sensing cyanide in water samples [23].

Despite these breakthroughs, most of these fluorescent nanoprobe are single-signal mode, which result in lower

Electronic supplementary material The online version of this article (<https://doi.org/10.1007/s00604-019-3803-0>) contains supplementary material, which is available to authorized users.

✉ Jun Hu
hjzjut@zjut.edu.cn

¹ College of Chemical Engineering, Zhejiang University of Technology, Hangzhou 310014, People's Republic of China

sensitivity, especially in contrast with organic fluorescent probes-based methods. Furthermore, a key challenge in developing nanoprobe for detecting cyanide in real samples is the lack of an effective means of converting specific cyanide binding into a rapid, visual readout. Ratiometric technique with self-calibration ability not only has been applied to improve the sensitivity but also realize visual identification in nanoprobe-based fluorescence methods [24, 25]. Constructing ratiometric nanoprobe commonly requires two individual fluorescence materials, one as a reference and the other as a response signal. An effective method is to couple fluorophores directly with another kind of one coated with silica shell [26–28]. However, the linked fluorophores on the surface of the silica usually suffer a great destruction during the assembly process, and the resultant nanoparticle is hard to control for ideal color change. In addition, complicated operation and low yield impede the massive use in real detection [29, 30]. To address these problems, researchers have geared their efforts toward developing new methods to realize ratiometric analysis by mixing the different types of fluorescent nanoparticles [31–33]. For example, Zhang's group reported a fluorescent ratiometric nanoprobe based on mixed QDs and CDs for visualization of arsenic(III).

Here we report a new method for the ratiometric detection of cyanide in drinking water and food samples with high sensitivity and excellent selectivity. The highly luminescent CDs and BSA-AuNCs were both synthesized by eco-friendly and low-cost methods. The ratiometric detection system was then constructed by mixing these two fluorophores upon optimized conditions. As shown in Scheme 1, BSA-AuNCs can selectively react with cyanide and form stable complex through strong covalent bonding, causing the fluorescence quenching. The CDs inside the system are only performed as a reference signal due to the electrostatic repulsion to cyanide. On these bases, we successfully demonstrated cyanide detection in aqueous solution within two-stage concentration and a detection limit as low as 8 nM is achieved. Besides, the present strategy has been

well-applied to quantitative detection and visual discrimination of cyanide in real samples.

Experimental

Reagents and apparatus

All the reagents and apparatus information used in experiments are given in the Electronic Supporting Material (ESM).

Synthesis of carbon dots (CDs) and BSA-AuNCs

Blue-emitting CDs and red-emitting BSA-AuNCs were prepared according to the reported methods [34, 35]. The details have been given in the ESM.

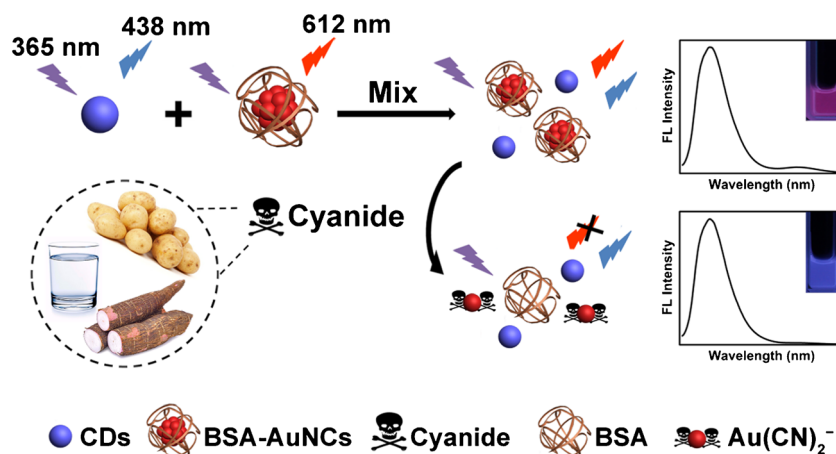
Standard procedures for determination of cyanide in buffer

In a typical fluorescent assay in aqueous buffer, the CDs (40 μL) and BSA-AuNCs (100 μL) were mixed in 760 μL of Na_2CO_3 -NaOH buffer (pH 12.0, 10 mM) at room temperature. The volumes of the CDs and BSA-AuNCs were fixed and the fluorescence intensity ratio of BSA-AuNCs to CDs was maintained as 1:20 to obtain the most obvious emission color change interval for visual detection. Then, different concentrations of cyanide (100 μL , 0–75 μM) were added to the above mixed solution. After incubated for 10 min, the fluorescence spectra were recorded at the excitation of 365 nm with the slit width of 10 nm.

Determination of cyanide in real samples

The samples of tap water collected at laboratory were filtered through a 0.22 μm membrane to remove solid suspensions. The samples of vegetables were prepared according to the

Scheme 1 Schematic diagram of the ratiometric detection system and the visual detection for cyanide



previous reports with a few modifications [36, 37]. First, cassava roots (2 g) and sprouted potatoes (2 g) were cut into small pieces and homogenized with a pestle and mortar. Then, the samples were incubated in a sealed beaker at room temperature for 1 h to enzymatically hydrolyze the cyanogenic glycoside. Then 5 mL deionized water was added to the above samples, and the mixture was centrifuged at 6000 rpm (10,196 g) for 10 min. The resultant supernatant was filtered using 0.22 μm filters and diluted to the detection range with $\text{Na}_2\text{CO}_3\text{-NaOH}$ buffer (pH 12.0, 10 mM). The procedure for treating liquor was as follows. Sodium hydroxide solution (5 mL, 2 $\text{g}\cdot\text{L}^{-1}$) was added to 1.0 mL liquor sample under vigorous stirring. After 10 min, the mixture was heated at 120 $^\circ\text{C}$ until approximately 1 mL of solution remained, and then cooled down to room temperature. The solution was redispersed in 10.0 mL of hydroxide solution (2 $\text{g}\cdot\text{L}^{-1}$) for further use. The pretreated samples spiked with different concentrations of cyanide were injected to the testing solution, and their fluorescence spectra were analyzed using the same procedure as above.

Results and discussion

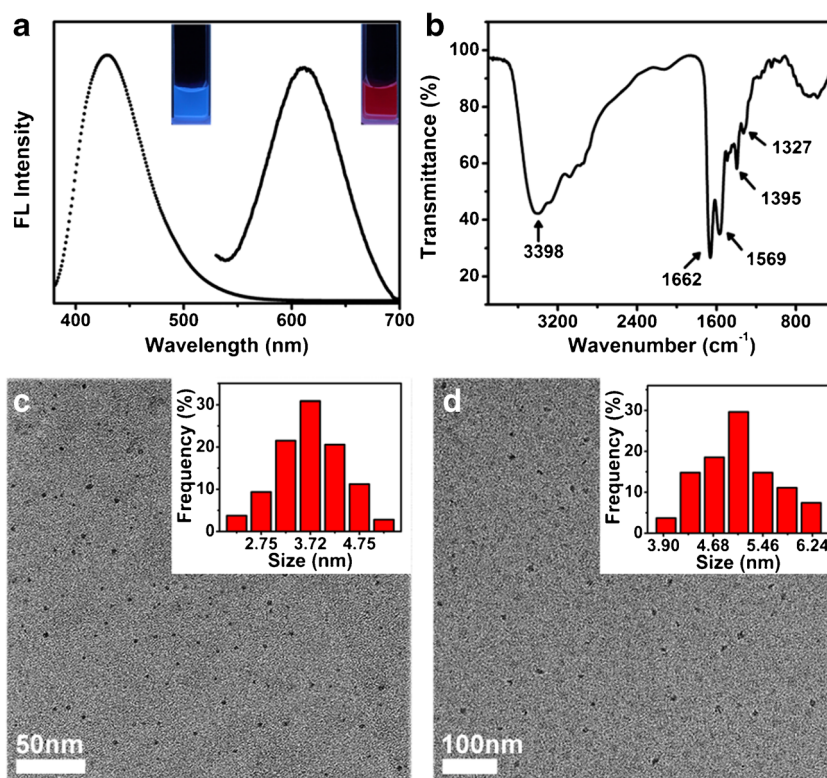
Characterization of CD/AuNC system

Fig. 1a reveals the fluorescence emission peak of CDs (dot line) at 438 nm, and the maximum emission center of AuNCs (solid line) at 612 nm, corresponding to bright blue and red fluorescence under the illumination of 365 nm UV light, respectively (insets of Fig. 1a).

The FT-IR spectrum was studied to identify the functional groups modified on the surface of CDs. As shown in Fig. 1b, the band at 3398 cm^{-1} is attributed to N–H and O–H stretching vibration, and peak at 1569 cm^{-1} is ascribed to N–H bending vibration. The stretching vibration of C–N appears at 1327 cm^{-1} . Other vibrations at 1662 cm^{-1} and broad band ranging from 3200 to 2800 cm^{-1} belong to conjugated C=O and O–H of associating carboxyl, respectively. These results elucidate the existence of the carboxyl and the amide groups on the surface of CDs [34, 38]. TEM images were taken to characterize the morphologies and sizes of the two components. The results illustrate both CDs and AuNCs (Fig. 1c, d) are nearly spherical and monodispersed, and their average sizes are estimated to be 3.75 ± 0.69 nm and 5.06 ± 0.71 nm, respectively.

The CD/AuNCs ratiometric detection system was constructed by mixing CDs and BSA-AuNCs with a certain fluorescence intensity ratio. As seen in Fig. S1, the mixed CDs and BSA-AuNCs are well dispersed in aqueous solution. Before adding cyanide, the fluorescence spectrum of the ratiometric system exhibits two characteristic emission peaks at 438 and 612 nm, which are donated by the band emission of CDs and BSA-AuNCs, respectively (Fig. 2). Simultaneously, a red fluorescence of the CD/AuNCs system is observed under a 365 nm UV light (a in Fig. 2). After the addition of cyanide, the emission of the CDs

Fig. 1 **a** Fluorescence emission spectra ($\lambda_{\text{ex}} = 365$ nm) of CDs (dot line) and BSA-AuNCs (solid line), insets are fluorescence photos of CDs (left) and BSA-AuNCs (right) under a 365 nm UV lamp. **b** FTIR spectrum of CDs. TEM images of CDs (c) and BSA-AuNCs (d) with their size distributions analysis (107 and 75 particles are measured respectively to analyze the size distribution)



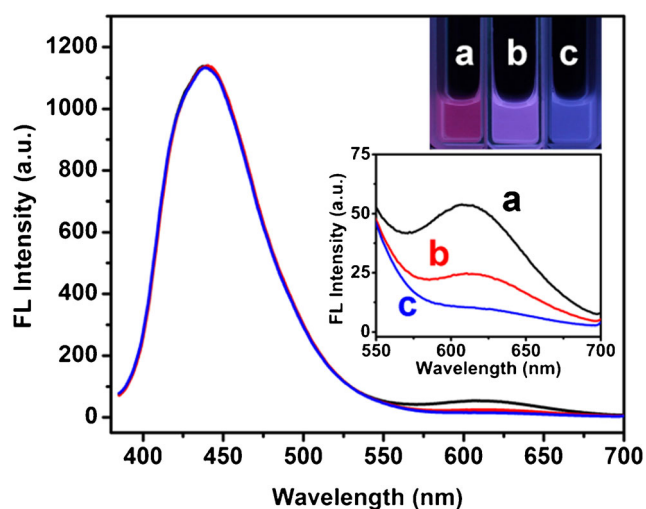


Fig. 2 Fluorescence emission spectra ($\lambda_{\text{ex}} = 365 \text{ nm}$) of CD/AuNCs system in the presence of (a) 0, (b) 5, and (c) 25 μM cyanide respectively. Insets: corresponding fluorescence photos under a 365 nm UV lamp

remains constant. This indicates that there is no obvious interaction between cyanide and CDs on the account of the repellent from negative charged surface and insensitivity to cyanide (Fig. S2). Contrastively, the fluorescence intensity of BSA-AuNCs obviously decreases, leading to a color changes from red to blue under the UV light (b and c in Fig. 2). Base on the fact, we presented a ratiometric fluorescence method for the visual determination of cyanide.

Optimization of method

The following parameters were optimized: (a) Sample pH value; (b) Reaction time; (c) Fluorescence intensity ratio. Respective data and Figures are given in the [ESM](#). The following experimental conditions were found to give best results: (a) Best sample pH value: 12.0 ($\text{Na}_2\text{CO}_3\text{-NaOH}$ buffer, 10 mM); (b) Optimal reaction time: 10 min; (c) Fluorescence intensity ratio: $I_{612}/I_{438} = 1:20$.

Determination of cyanide

The assay was applied to determine cyanide under the optimal experimental condition. The emission intensity of BSA-AuNCs at 612 nm decreases continuously with the increasing concentration of cyanide, the reference fluorescence intensity of CDs at 438 nm is almost unchanged (Fig. 3a). As presented in Fig. 3b, the fluorescence intensity ratios ($(I_{612}/I_{438})_0/(I_{612}/I_{438})$) exhibit two linear responses to the cyanide concentration in the range of 8 nM–12.5 μM and 12.5–75 μM with the correlation coefficient (R^2) of 0.9995 and 0.9994, respectively. The detection limit is calculated to be as low as 8 nM ($S/N =$

3). The related Stern–Volmer equation can be described as follow:

$$(I_{612}/I_{438})_0/(I_{612}/I_{438}) = 1 + K_{\text{sv}} [Q] \quad (1)$$

From the slope of the insets in Fig. 3b, the K_{sv} values are estimated to be $2.37 \times 10^5 \text{ mol}^{-1}\cdot\text{L}$ and $9.15 \times 10^4 \text{ mol}^{-1}\cdot\text{L}$, indicating the strong quenching efficiency of BSA – AuNCs with cyanide. The fluorescence lifetime of BSA – AuNCs is less than 1.84 μs [39, 40]. According to the $K_q = K_{\text{sv}}/\tau$, the values of emission quenching constant (K_q) are $1.29 \times 10^{11} \text{ L}\cdot\text{mol}^{-1}\cdot\text{s}^{-1}$ and $4.97 \times 10^{10} \text{ L}\cdot\text{mol}^{-1}\cdot\text{s}^{-1}$. The value of K_q is larger than the highest scattering collision quenching constant ($2.00 \times 10^{10} \text{ L}\cdot\text{mol}^{-1}\cdot\text{s}^{-1}$) [41], thus the reaction is static quenching process. Compared with reported works with respect to cyanide detection, this fluorescent method shows a comparable or even more sensitive response (Table S1). Fluorescence performance of single signal output was also investigated to clarify the advantage of visual assay with ratiometric fluorescence technique. The fluorescence color change of the single BSA-AuNCs is quite indistinguishable in contrast with our ratiometric method (inset of Fig. 3c). Furthermore, the fluorescence intensity of single BSA-AuNCs expresses a narrower linear relationship in the cyanide concentration ranging from 2.5 to 50 μM (Fig. 3d). The above results imply that the ratiometric fluorescence detection system is available in visual assay with higher credibility and sensitivity.

Selectivity

In cyanide detection system, the interference from other anions is also vital to the appliance of system detection. Therefore, we investigated the response of our method towards various anions, including SO_3^{2-} , Br^- , BrO_3^- , Cl^- , NO_3^- , oxalate $^{2-}$, SCN^- , SO_4^{2-} , I^- , IO_4^- , CO_3^{2-} , PO_4^{3-} , acetate $^-$, F^- , NO_2^- , $\text{B}_4\text{O}_7^{2-}$, malate $^{2-}$ and citrate $^{3-}$. As showed in Fig. 4a, the fluorescence intensity ratio ($(I_{612}/I_{438})_0/(I_{612}/I_{438})$) increases obviously when 5 μM cyanide is added to the solution. Sulfate ions cause the slight fluorescence quenching of BSA-AuNCs, in accompaniment with the color changes into dark purple (inset of Fig. 4a). Periodate ions quench both CDs and BSA-AuNCs to some degree. This causes a minor change of fluorescence intensity ratio and a slightly darker color. Besides, the ratio decreases in the high concentration of carbonate (more than 10 mM) due to the fluorescence enhancement of BSA-AuNCs and quenching effect of the CDs. Other anions do not cause obvious emission change, demonstrating the excellent selectivity of the method for cyanide. The interference experiment was also examined by introducing related co-exist anions (Fig. 4b). When 20-fold interfering anions (100 μM) are added to the detection solution, no appreciable changes are observed. After injecting cyanide to the

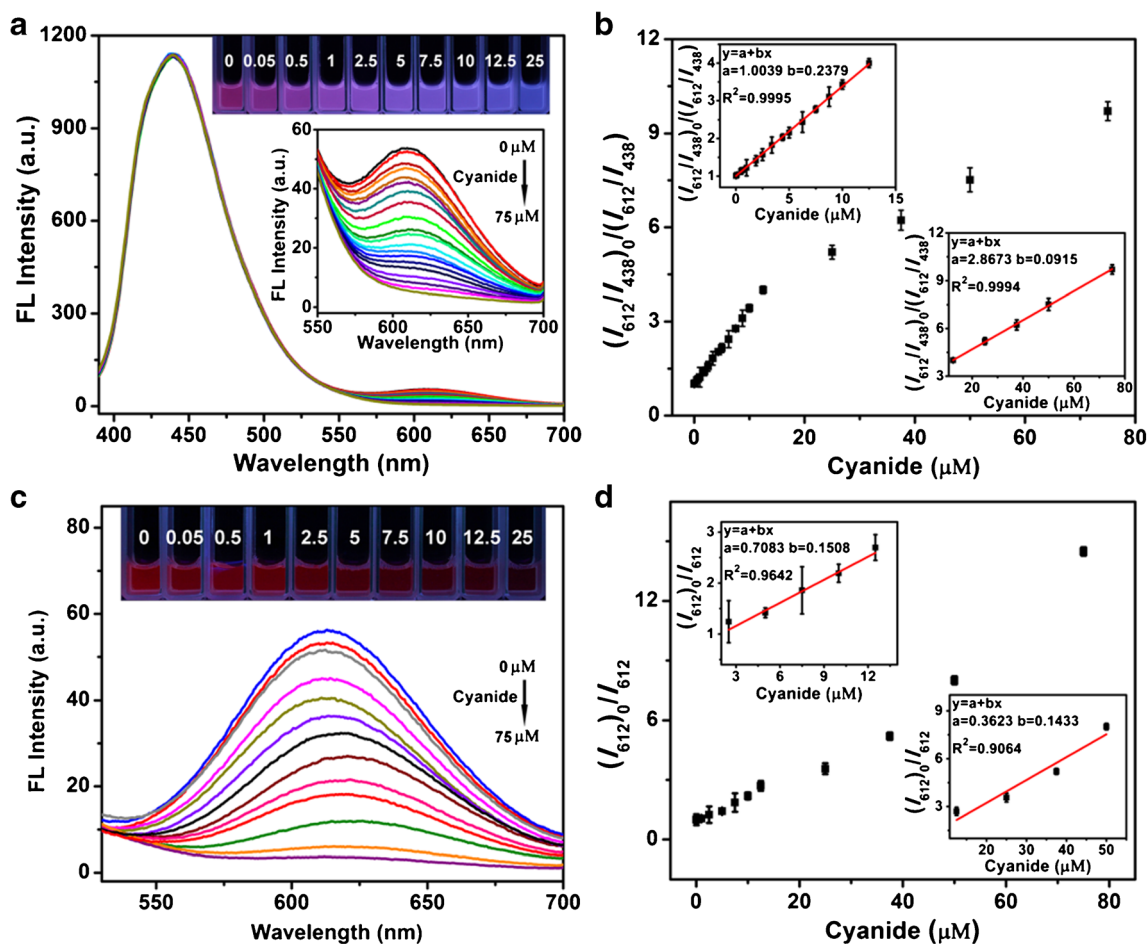


Fig. 3 **a** Fluorescence spectra of the CD/AuNCs system with increasing concentration of cyanide ($\lambda_{\text{ex}} = 365$ nm), insets are corresponding fluorescence photos under 365 nm UV lamp. **b** The linear calibration plots (CD/AuNCs system) of the fluorescence intensity ratios ($(I_{612}/I_{438})_0/(I_{612}/I_{438})$) in the range of 8 nM—75 μM cyanide. **c** Fluorescence

spectra of the pure BSA-AuNCs exposed to cyanide ($\lambda_{\text{ex}} = 365$ nm), insets images are related fluorescence photos taken under 365 nm UV lamp. **d** The linear calibration plots (pure BSA-AuNCs) of the fluorescence intensity toward concentration of cyanide

interfering anions existed solution, the fluorescence quenches obviously, which is almost equivalent to the case of adding individual cyanide. The results demonstrate our method can identify cyanide from other co-existed anions.

Sensing mechanism

According to the literature, the optical performances of BSA-AuNCs are extremely size-dependent, protein-stabilized, and related to the chemical state of the Au atoms [41]. Upon the addition of cyanide, the fluorescence intensity of BSA-AuNCs decreases through the etching and formation of $\text{Au}(\text{CN})_2^-$ complexes [42]. ICP-MS was performed to confirm the etching process by comparing with the content of Au in BSA-AuNCs in the absence and presence of cyanide. To rule out the interference of $\text{Au}(\text{CN})_2^-$, ultrafiltration was carried on before the analysis. The amount of Au in the aqueous solution of pure BSA-AuNCs reaches $1003 \mu\text{g}\cdot\text{mL}^{-1}$. After the reaction with

cyanide, only $0.53 \mu\text{g}\cdot\text{mL}^{-1}$ of Au is contained in the AuNCs (Table S2). The result illustrates the dissolution of Au atoms in the BSA-AuNCs by cyanide. To get further insight into the quenching mechanism, the excitation spectra of the BSA-AuNCs and CD/AuNCs system with incremental concentration of cyanide were investigated (Fig. S7). The typical excitation peaks located at 370 nm of pure BSA-AuNCs and CD/AuNCs system are both decreased when 5 and 50 μM cyanide are injected. We find that the excitation intensity decreases by 44.3% after adding 5 μM cyanide, the intensity reduction is estimated only 41% upon the concentration of cyanide changing from 5 to 50 μM . These two-stage changes of intensity correspond to the trend of the two linear responses to the cyanide concentration in fluorescence emission spectra (Fig. 3b). We ascribe these two different quenching efficiency of detection system to the surface Au(I) atomic and Au(0) core of BSA-AuNCs [43], which react with cyanide through two different ways. Cyanide can strongly

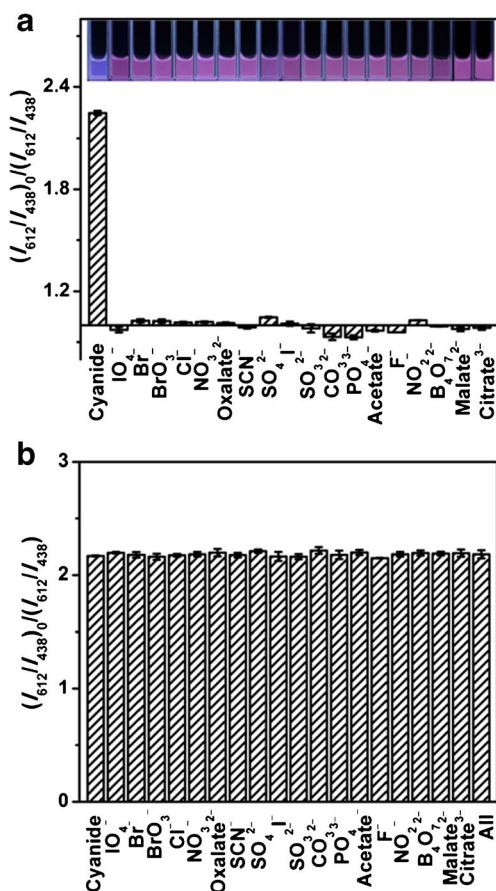
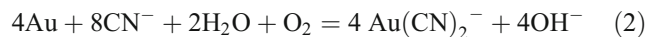


Fig. 4 Selectivity (a) and interference studies (b) of the CD/AuNCs system toward different anions in Na_2CO_3 -NaOH buffer (pH 12.0, 10 mM). All investigated anions were 0.1 mM. The inset photos were taken under the 365 nm UV lamp

coordinate with the Au(I) on the surface of BSA-AuNCs, and the fluorescence intensity decreases rapidly along with the formation of $\text{Au}(\text{CN})_2^-$ [44]. Upon the increasing

amount of cyanide, BSA-AuNCs are further quenched via the oxidation of Au(0) in the core of BSA-AuNCs, which is reported as Elsner reaction [45].



The hypothesis was verified by XPS characterization. Fig. 5a shows that the Au 4f_{7/2} spectrum can be deconvoluted into two types of peaks located at 84.0 and 85.1 eV. These correlate to Au(0) and Au(I) (contained 12%) of pure BSA-AuNCs respectively [45, 46]. When 5 μM of cyanide is injected, the fluorescence intensity of the BSA-AuNCs is obviously weakened with the quenching efficiency to 54%, the Au(I) peak at 85.1 eV resulted by the oxidation of Au(0) enhances slightly (Fig. 5b, Table S3), indicating that the main cause of the fluorescence response in the early stage is the coordination of the Au(I) on the surface of BSA-AuNCs. As the amount of cyanide increases, the Au(0) peak completely disappears and only the enhanced Au(I) peak at 85.1 eV can be observed, indicating all the Au atoms in the Au NCs are oxidized by cyanide in the second stage. Moreover, the high resolution XPS spectra of N1 s peaks were performed to analyze the chemical state of N (Fig. 5d-f). The N1 s peak centered at 399.6 eV is attributed to the nitrogen atoms of BSA [47, 48]. With the increasing of cyanide, a peak significantly appears at 397.9 eV in Fig. 5f, which is assigned to CNO^- [49]. We attribute this appearance to the oxidation and negative consumption of cyanide. During the oxidation reaction caused dissolution process in the second stage, H_2O_2 is produced as an intermediate production according to Bodländer reaction [50].

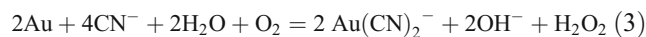


Fig. 5 XPS spectra of Au 4f (a-c) and N 1s (d-f) peaks for the BSA-AuNCs in the absence of cyanide (a, d), in the presence of 5 (b, e) and 100 μM cyanide (c, f)

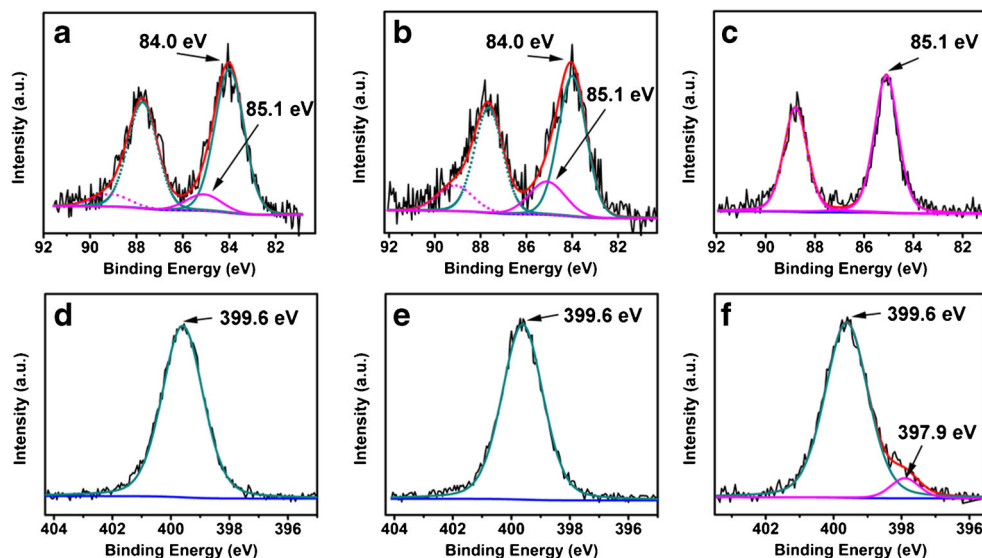
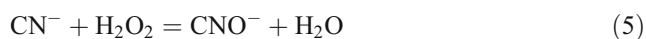


Table 1 Applications of the CD/AuNCs system in real samples ($n = 5$)

Samples	Initial amount	Added cyanide (μM)	Standard detected (μM)	Recovery (%)
Roots of cassava	$77.35 \pm 5.09 \text{ mg}\cdot\text{kg}^{-1}$	0	1.19 ± 0.07	–
		0.5	1.69 ± 0.02	101.6 ± 3.2
		2.0	3.17 ± 0.05	98.8 ± 3.1
		6.0	7.12 ± 0.96	99.8 ± 2.8
Sprouted potatoes	$6.60 \pm 0.45 \mu\text{g}\cdot\text{kg}^{-1}$	0	0.16 ± 0.01	–
		0.5	0.65 ± 0.02	100.5 ± 3.3
		2.0	2.14 ± 0.06	99.3 ± 2.6
		6.0	6.19 ± 0.15	100.1 ± 2.5
Tap water	ND ^a	0.5	0.49 ± 0.01	99.9 ± 2.5
		2.0	2.03 ± 0.04	100.8 ± 2.1
		6.0	6.04 ± 0.12	100.6 ± 2.0
Liquor	ND ^a	0.5	0.51 ± 0.06	100.1 ± 3.9
		2.0	1.95 ± 0.14	97.9 ± 2.7
		6.0	6.02 ± 0.28	100.4 ± 3.3

^a Not Detectable

Due to the presence of H_2O_2 , cyanide in alkaline solution is converted to CNO^- [51–53], which lose the ability to react with BSA-AuNCs and have no effect to the fluorescence intensity of CD/AuNCs system. The reaction equation is as follows.

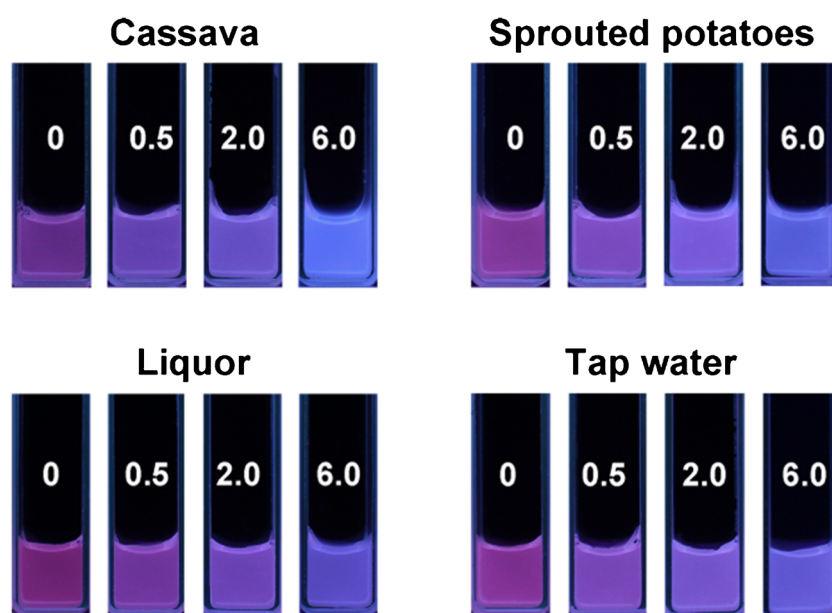


Compared to the direct coordination step, the oxidation reaction caused etching process and negative consumption of cyanide lead to the more gentle decrease of fluorescence intensity.

Determination of cyanide in real samples

The feasibility was evaluated for detecting cyanide in real samples, including tap water, cassava roots, sprouted potatoes and liquor using the ratiometric fluorescence method. In order to study the effects of sample matrix on the analysis system, the standard addition method was carried on via adding different amounts of cyanide (0.5, 2.0 and 6.0 μM) to pretreated samples. The recovery and analytical results are listed in Table 1. The recoveries of these pretreated samples are among 95.0% to 104.7%, which meet the need of quantitative analysis in the real

Fig. 6 Visual detection of cyanide in real samples by the CD/AuNCs system spiked with 0, 0.5, 2.0 and 6.0 μM cyanide, respectively



samples. Additionally, the fluorescence pictures for the visual detection of cyanide were taken to check its practical applicability as on-site detection kit (Fig. 6). It can be seen the detection solution impregnated with different amounts of cyanide emitted red-purple-blue luminescence under 365 nm UV lamp illumination, and the emission color changes can be identified visually. It is worth mentioning that CD/AuNCs system is designed to work in Na₂CO₃-NaOH buffer (10 mM), thus the method is applicable for pretreated samples that contain the concentration of carbonate less than 10 mM. These results demonstrate that this ratiometric method can be used for visual assay of cyanide in real samples.

Conclusions

A ratiometric system was constructed by mixing of two different nanoparticles, and this method has been established for quantitative detection of cyanide on the basis of the measurement of fluorescence intensity ratios. The nanoprobe can also be used to visual discrimination of cyanide, the existence and content of cyanide can be recognized by the fluorescence color change of the nanoprobe. The platform shows excellent sensitivity and selectivity for cyanide, and its utility as an on-site testing reagent has been demonstrated in food, drink and water samples. Besides, the possible mechanism of the two linear responses on account of surface Au(I) atomic and Au(0) core of BSA-AuNCs was investigated in detail. We expect that this work will pave the way for the development of visual detection of cyanide using eco-friendly method in the future.

Acknowledgements The authors gratefully acknowledge the financial support from National Natural Science Foundation of China (21875218, 21501191, 51672248 and 51872261) and Zhejiang Provincial Natural Science Foundation (LR19E020002).

Compliance with ethical standards

Conflict of interest The author(s) declare that they have no competing interests.

References

- Wang F, Wang L, Chen X, Yoon J (2014) Recent progress in the development of fluorometric and colorimetric chemosensors for detection of cyanide ions. *Chem Soc Rev* 43:4312–4324
- Chen Q, Zhu L, Chen J, Jiang T, Ye H, Ji H, Tsang S, Zhao Z, Yi T, Chen H (2019) Recent progress in nanomaterial-based assay for the detection of phytotoxins in foods. *Food Chem* 277:162–178
- Mu JJ, Feng QY, Chen XD, Li J, Wang HL, Li MJ (2015) Silica nanoparticles doped with an iridium(III) complex for rapid and fluorometric detection of cyanide. *Microchim Acta* 182:2561–2566
- Hallaj R, Haghghi N (2017) Photoelectrochemical amperometric sensing of cyanide using a glassy carbon electrode modified with graphene oxide and titanium dioxide nanoparticles. *Microchim Acta* 184:3581–3590
- Amjadi M, Hassanzadeh J, Manzoori JL (2014) Determination of cyanide using a chemiluminescence system composed of permanganate, rhodamine B, and gold nanoparticles. *Microchim Acta* 181: 1851–1856
- Li Z, Liu C, Wang SJ, Xiao LW, Jing XM (2019) Visual detection of cyanide ion in aqueous medium by a new chromogenic azo-azomethine chemosensor. *Spectrochim Acta A* 210:321–328
- Niu QF, Lan LX, Li TD, Guo ZR, Jiang T, Zhao ZY, Feng ZS, Xi JY (2018) A highly selective turn-on fluorescent and naked-eye colorimetric sensor for cyanide detection in food samples and its application in imaging of living cells. *Sensor Actuat B-Chem* 276: 13–22
- Dalapati R, Nandi S, Reinsch H, Bhunia BK, Mandal BB, Stock N, Biswas S (2018) Fluorogenic naked-eye sensing and live-cell imaging of cyanide by a hydrazine-functionalized CAU-10 metal-organic framework. *CrystEngComm* 20:4194–4201
- Long LL, Huang MY, Wang N, Wu YJ, Wang K, Gong AH, Zhang ZJ, Sessler JL (2018) A mitochondria-specific fluorescent probe for visualizing endogenous hydrogen cyanide fluctuations in neurons. *J Am Chem Soc* 140:1870–1875
- Maity D, Vyas G, Bhatt M, Paul P (2015) Detection of NaCN in aqueous media using a calixarene-based fluoroionophore containing ruthenium(II)-bipyridine as the fluorogenic unit. *RSC Adv* 5: 6151–6159
- Qing Z, Hou L, Yang L, Zhu L, Yang S, Zheng J, Yang R (2016) A reversible nanolamp for instantaneous monitoring of cyanide based on an Elsner-like reaction. *Anal Chem* 88:9759–9765
- Wang Y, Kim SH, Feng L (2015) Highly luminescent N, S-codoped carbon dots and their direct use as mercury(II) sensor. *Anal Chim Acta* 890:134–142
- Bagheri N, Djafarzadeh N, Hassanzadeh J (2016) Inhibition of rhodamine B-ferricyanide chemiluminescence by gold nanoparticles and sensitive determination of hazardous cyanide. *Anal Sci* 32: 317–322
- Lien CW, Unnikrishnan B, Harroun SG, Wang CM, Chang JY, Chang HT, Huang CC (2018) Visual detection of cyanide ions by membrane-based nanozyme assay. *Biosens Bioelectron* 102: 510–517
- Lou YB, Zhao YX, Zhu JJ (2016) Ultrasensitive optical detection of anions by quantum dots. *Nanoscale Horiz* 1:125–134
- Lim SJ, Ma L, Schleife A, Smith AM (2016) Quantum dot surface engineering: toward inert fluorophores with compact size and bright, stable emission. *Coord Chem Rev* 320:216–237
- Wu P, Zhao T, Wang SL, Hou XD (2014) Semiconductor quantum dots-based metal ion probes. *Nanoscale* 6:43–64
- Ding CQ, Zhu AW, Tian Y (2014) Functional surface engineering of C-dots for fluorescent biosensing and in vivo bioimaging. *Acc Chem Res* 47:20–30
- Wang J, Li RS, Zhang HZ, Wang N, Zhang Z, Huang CZ (2017) Highly fluorescent carbon dots as selective and visual probes for sensing copper ions in living cells via an electron transfer process. *Biosens Bioelectron* 97:157–163
- Zhang LB, Wang EK (2014) Metal nanoclusters: new fluorescent probes for sensors and bioimaging. *Nano Today* 9:132–157
- Wu JP, Jiang KL, Wang XJ, Wang CX, Zhang C (2017) On-off-on gold nanocluster-based near infrared fluorescent probe for recognition of Cu(II) and vitamin C. *Microchim Acta* 184:1315–1324
- Tian L, Li YF, Ren TT, Tong YL, Yang BS, Li YQ (2017) Novel bimetallic gold-silver nanoclusters with "synergy"-enhanced fluorescence for cyanide sensing, cell imaging and temperature sensing. *Talanta* 170:530–539
- Wang CW, Chen YN, Wu BY, Lee CK, Chen YC, Huang YH, Chang HT (2016) Sensitive detection of cyanide using bovine

- serum albumin-stabilized cerium/gold nanoclusters. *Anal Bioanal Chem* 408:287–294
24. Long Y, Zhou J, Yang MP, Liu XJ, Zhang M, Yang BQ (2016) Highly selective, sensitive and naked-eye fluorescence probes for the direct detection of hypochlorite anion and their application in biological environments. *Sensor Actuat B-Chem* 232:327–335
25. Chen AM, Peng X, Pan ZF, Shao K, Wang J, Fan MH (2018) Visual assay of glutathione in vegetables and fruits using quantum dot ratiometric hybrid probes. *J Agric Food Chem* 66:6431–6438
26. Huang XY, Zhou YJ, Liu C, Zhang RL, Zhang LY, Du SH, Liu BH, Han MY, Zhang ZP (2016) A single dual-emissive nanofluorophore test paper for highly sensitive colorimetry-based quantification of blood glucose. *Biosens Bioelectron* 86:530–535
27. Wang J, Peng X, Li DQ, Jiang XC, Pan ZF, Chen AM, Huang L, Hu J (2018) Ratiometric ultrasensitive fluorometric detection of ascorbic acid using a dually emitting CdSe@SiO₂@CdTe quantum dot hybrid. *Microchim Acta* 185:42–50
28. Yan YH, Sun J, Zhang K, Zhu HJ, Yu H, Sun MT, Huang DJ, Wang SH (2015) Visualizing gaseous nitrogen dioxide by ratiometric fluorescence of carbon nanodots-quantum dots hybrid. *Anal Chem* 87:2087–2093
29. Snee PT (2018) The role of colloidal stability and charge in functionalization of aqueous quantum dots. *Acc Chem Res* 51:2949–2956
30. Wang J, Ma M, Huang RB, Wang LG, Chen AM, Hu J (2015) An efficient ratiometric fluorescent probe based on dual-emission fluorescent silica nanoparticles for visual determination of Hg²⁺. *Anal Methods* 7:2295–2299
31. Zhou YJ, Huang XY, Liu C, Zhang RL, Gu XL, Guan GJ, Jiang CL, Zhang LY, Du SH, Liu BH, Han MY, Zhang ZP (2016) Color-multiplexing-based fluorescent test paper: dosage-sensitive visualization of arsenic(III) with discernable scale as low as 5 ppb. *Anal Chem* 88:6105–6109
32. Wang XY, Yu SM, Liu W, Fu LW, Wang YQ, Li JH, Chen LX (2018) Molecular imprinting based hybrid ratiometric fluorescence sensor for the visual determination of bovine hemoglobin. *ACS Sens* 3:378–385
33. Liu X, Li B, Xu Y, Li ZQ, Zhang Y, Ding ZJ, Cui H, Wang J, Hou HB, Li HR (2019) A highly selective lanthanide-containing probe for ratiometric luminescence detection of an anthrax biomarker. *Dalton Trans* 48:7714–7719
34. Xu SF, Lu HZ (2016) Mesoporous structured MIPs@CDs fluorescence sensor for highly sensitive detection of TNT. *Biosens Bioelectron* 85:950–956
35. Tao Y, Lin YH, Ren JS, Qu XG (2013) A dual fluorometric and colorimetric sensor for dopamine based on BSA-stabilized Au nanoclusters. *Biosens Bioelectron* 42:41–46
36. Liu C-Y, Tseng W-L (2012) Using polysorbate 40-stabilized gold nanoparticles in colorimetric assays of hydrogen cyanide in cyanogenic glycoside-containing plants. *Anal Methods* 4:2537–2542
37. Mannel-Croise C, Probst B, Zelder F (2009) A straightforward method for the colorimetric detection of endogenous biological cyanide. *Anal Chem* 81:9493–9498
38. Zhu SJ, Meng QN, Wang L, Zhang JH, Song YB, Jin H, Zhang K, Sun HC, Wang HY, Yang B (2013) Highly photoluminescent carbon dots for multicolor patterning, sensors, and bioimaging. *Angew Chem Int Ed* 52:3953–3957
39. Raut S, Chib R, Rich R, Shumilov D, Gryczynski Z, Gryczynski I (2013) Polarization properties of fluorescent BSA protected Au₂₅ nanoclusters. *Nanoscale* 5:3441–3446
40. Chevrier DM, Thanthirige VD, Luo Z, Driscoll S, Cho P, MacDonald MA, Yao Q, Guda R, Xie J, Johnson ER, Chatt A, Zheng N, Zhang P (2018) Structure and formation of highly luminescent protein-stabilized gold clusters. *Chem Sci* 9:2782–2790
41. Rajamanikandan R, Ilanchelian M (2018) Protein-localized bright-red fluorescent gold nanoclusters as cyanide-selective colorimetric and fluorometric nanoprobe. *ACS Omega* 3:14111–14118
42. Wei SC, Hsu PH, Lee YF, Lin YW, Huang CC (2012) Selective detection of iodide and cyanide anions using gold-nanoparticle-based fluorescent probes. *ACS Appl Mater Interfaces* 4:2652–2658
43. Liu CL, Wu HT, Hsiao YH, Lai CW, Shih CW, Peng YK, Tang KC, Chang HW, Chien YC, Hsiao JK, Cheng JT, Chou PT (2011) Insulin-directed synthesis of fluorescent gold nanoclusters: preservation of insulin bioactivity and versatility in cell imaging. *Angew Chem Int Ed* 50:7056–7060
44. Lu DT, Liu LL, Li FX, Shuang SM, Li YF, Choi MMF, Dong C (2014) Lysozyme-stabilized gold nanoclusters as a novel fluorescence probe for cyanide recognition. *Spectrochim Acta A* 121:77–80
45. Liu Y, Ai K, Cheng X, Huo L, Lu L (2010) Gold-nanocluster-based fluorescent sensors for highly sensitive and selective detection of cyanide in water. *Adv Funct Mater* 20:951–956
46. Xie JP, Zheng YG, Ying JY (2009) Protein-directed synthesis of highly fluorescent gold nanoclusters. *J Am Chem Soc* 131:888–889
47. Song SW, Hidajat K, Kawi S (2005) Functionalized SBA-15 materials as carriers for controlled drug delivery: influence of surface properties on matrix-drug interactions. *Langmuir* 21:9568–9575
48. Peng ZG, Hidajat K, Uddin MS (2004) Adsorption of bovine serum albumin on nanosized magnetic particles. *J Colloid Interface Sci* 271:277–283
49. Folkesson B (1973) ESCA studies on the charge distribution in some dinitrogen complexes of rhenium, iridium, ruthenium, and osmium. *Acta Chem Scand* 27:287–302
50. Bodläender G (1896) Die chemie des cyanidverfahrens. *Angew Chem* 9:583–587
51. Chen FY, Zhao X, Liu HJ, Qu JH (2014) Reaction of Cu(CN)₃²⁻ with H₂O₂ in water under alkaline conditions: cyanide oxidation, Cu⁺/Cu²⁺ catalysis and H₂O₂ decomposition. *Appl Catal B Environ* 158:85–90
52. Sarla M, Pandit M, Tyagi DK, Kapoor JC (2004) Oxidation of cyanide in aqueous solution by chemical and photochemical process. *J Hazard Mater* 116:49–56
53. Wiggins-Camacho JD, Stevenson KJ (2011) Indirect electrocatalytic degradation of cyanide at nitrogen-doped carbon nanotube electrodes. *Environ Sci Technol* 45:3650–3656